Document downloaded from:

http://hdl.handle.net/10251/101890

This paper must be cited as:

The final publication is available at

http://doi.org/10.1016/j.tsf.2017.06.001

Copyright Elsevier

Additional Information

Autor version: A. Urbaniak, M. Pawłowski, M. Marzantowicz, T. Sall and **B. Marí;** *Thin Solid Films 636, 158-163 (2017) https://doi.org/10.1016/j.tsf.2017.06.001*

Opto-electrical characterization of In doped SnS thin films for photovoltaic applications

A. Urbaniak[1], M. Pawłowski[1], M. Marzantowicz[1], T. Sall[2], B. Marí[2]

[1]Faculty of Physics, Warsaw University of Technology, Koszykowa 75, PL 00 662 Warszawa, Poland

[2]Insitut de Disseny i Fabricació, Universitat Politècnica de València, Cami de Vera s/n, 46022 Valencia, Spain

Abstract

Spray pyrolised SnS thin films doped with indium were studied using various optical and electrical techniques. Structural analysis shows that all films crystallize in orthorhombic structure with (111) as a preferential direction without secondary phases. Doping of SnS layers with indium results in better morphology with increased grain size. Absorption measurements indicate dominant direct transition with energy decreasing from around 1.7 eV to 1.5 eV with increased indium supply. Apart from direct transition, an indirect one, of energy of around 1.05 eV, independent on indium doping was identified. The photoluminescence study revealed two donors to acceptor transitions between two deep defect levels and one shallower with energy of around 90 meV. The observed transitions did not depend significantly on In concentration. The conductivity measurements reveal thermal activation of conductivity with energy decreasing from around 165 meV to 145 meV with increased In content.

Introduction

The thin film photovoltaic's are nowadays dominated by CdTe and $Cu(In,Ga)Se_2$ based technologies [1,2]. However, the supply issues of In, Ga and Te as well as the toxicity and disposal requirements of Cd encourage search for other photovoltaic materials. Therefore, more simple, binary and Earth-abundant compounds like SnS [3], FeS_2[4] and Cu_2S [5] have recently received interest in the photovoltaic community. The SnS has high optical absorption of photons with energies above 1.3 eV [3,6], which is in the range of 1 eV – 1.5 eV considered as the bandgap energy boundaries for a optimum absorber in solar cells [7]. SnS shows an intrinsic p-type conductivity due to formation of tin vacancies V_{Sn} [3,6] with carrier concentrations above 10^{15} cm^{-3} [3]. Despite these promising electrical and optical parameters, efficiencies of SnS – based solar cells are far from satisfactory, with record efficiency of 4.36% [8]. Moreover, this record has been achieved using Atomic Layer Deposition, which is not a well scalable technique while considering a solar cell production beyond a laboratory scale.

Here we investigated SnS thin films made by a spray pyrolysis [9,10] – a simple, inexpensive and versatile technique suitable for industrial scale production. In this case, the obtained so far efficiencies are below 2% [3]. This could be due to intrinsic limitations of the material or due to the lack of proper material growth and device optimization. One of the important issues for an absorber material is control of its carrier concentration by either appropriate doping or growth parameters. Theoretical calculations [11] predict that an antisite defect In_{Sn} has low formation energy under S-rich growth conditions and should act as a shallow acceptor introducing holes into material. In the following work we have prepared In doped SnS thin films by spray pyrolysis [12, 13] and studied its basic optical and electrical properties.

Experimental

Thin films preparation

The SnS films were prepared using aqueous solution containing tin (II) chloride dehydrate ($SnCl_2 \cdot 2H_2O$), thiourea ($SC(NH_2)_2$). Indium chloride ($InCl_3$) was directly added to the solution at different concentrations. To avoid growth of Sn_2S_3 and SnS_2 phases, Sn (II) instead of Sn(IV) was used [14]. Thin films were grown on the glass substrate keeping the constant substrate temperature of 350°C. To obtain clean and stain-free substrates, an ultrasonic bath was used and substrates were immersed for 15 minutes in acetone solution bath, rinsed with distilled water, immersed in an ethanol bath solution, rinsed with distilled water before drying and use for deposition.

Thin films characterization

The X-Ray Diffraction (XRD) measurements were made using Rigaku Ultima IV diffractometer at the Bragg-Brentano (θ-2θ) configuration and with Cu:Kα radiation $(1.5418\ \text{Å})$. Atomic Force Microscope (AFM) analysis was carried out using NT-MDT NTEGRA PRIMA microscope in a semi contact mode. Optical properties including transmittance and reflectance were made using Bentham PVE300 setup in the 300 nm - 1800 nm range of light wavelength using a halogen and wolfram light source and Ge and Si photodetectors. The Photoluminescence (PL) was carried out using the lock-in technique. The samples were excited with 514.5 nm chopped Ar+ laser light in the laser power output range from 4 mW to 500 mW, which corresponds to the excitation density roughly from 100 mW/cm^2 to 12.5 W/cm^2. The PL signal was collected with an iHR550 grating monochromator and detected with a liquid nitrogen cooled germanium detector. Samples were cooled down to low temperatures in the helium closed-cycle setup and analyzed in the 10 K – 100 K temperature range. To perform electrical measurements Al electrodes were evaporated on SnS film in planar configuration. The conductivity was then measured in nitrogen cooled cryostat in the 80 K – 330 K temperature range.

Results and discussion

XRD analysis and AFM measurements

To investigate the crystalline properties of synthesized films XRD measurements were made together with AFM imaging. The diffraction spectra of all four SnS thin films are presented in Figure 1.

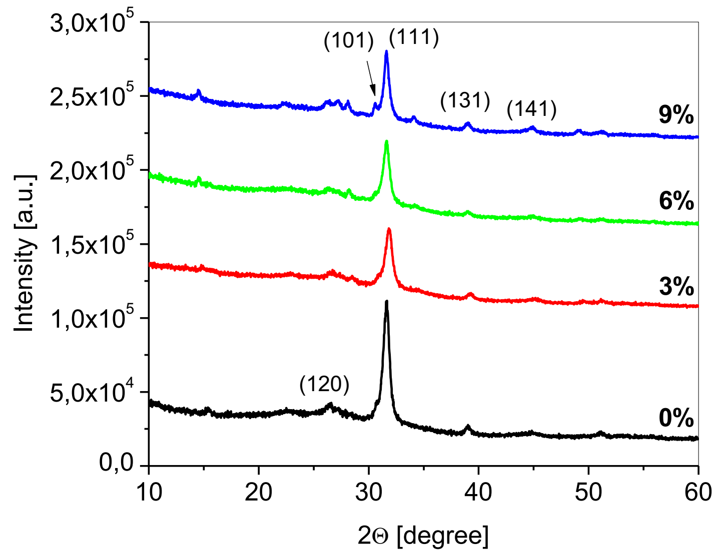

Figure 1. XRD spectra for SnS samples with different In concentration in the sprayed solution. Preferential crystallographic directions are included on the graph.

All films are polycrystalline and XRD peaks are in good agreement with standard data for SnS orthorhombic phase (JCPDS #39-0354) with (111) as the preferential crystallographic direction. The peaks are broad which indicates high disorder in the material as well as point into small crystallite sizes. The intensity of the (111) main peak decreases with increased amount of In. The crystallite size of SnS thin film doped with indium for the main (111) XRD peak can be calculated using Scherrer formula: $D=k\lambda/\beta\cos\theta$. Here D is the crystalline size, k is a crystallite shape factor being in the range of 0.62 – 2.08 [15] (k=0.9 was used), λ=1.5418 Å is the wavelength of x-ray radiation, β is the full width at half maximum (FWHM) of the Gaussian peak fitted to the data and θ is the Bragg angle of diffraction. To determine θ and FWHM parameters we used X'Pert HighScore software. Calculated crystallite sizes are presented in Table 1. Size of crystallites in investigated samples is in the range 116 Å – 125 Å and does not depend significantly on the amount of indium supplied during growth.
Figure 2 shows AFM images of investigated SnS thin films. The scan area was 8 μm x 8 μm wit 512 x 512 resolution. Films have irregular structure with longitudinal type of grains, which was already observed in spray pyrolised SnS thin films [10]. The average grain size and the average roughness height are presented in Table 1. The presence of indium during growth generally increases the mean grain size from around 38 nm to around 60 nm as well as the roughness of the film. However, there is no further increase of grain size when more indium is added.

The average grain size is also larger than the average crystallite size obtained from XRD. This might be a result of different physical meaning of calculated size parameters between XRD and AFM analysis. Scherrer equation gives the minimum crystallite size and the analysis of AFM provides the mean grain size. Taking into account that the grains are clearly longitudinal we might expect higher average grain size then the minimum crystallite width. The second reason might be the fact that the grains might actually consist of few smaller crystallites undistinguishable by AFM analysis.

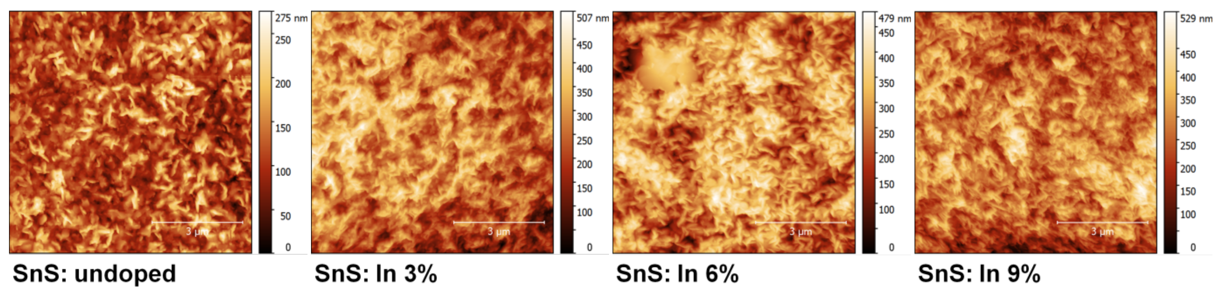

Figure 2. AFM images of SnS thin films deposited with different concentration of indium in the sprayed solution.

Table 1. Size of crystallites calculated from XRD spectra and grain parameters calculated based on the AFM images.

sample	crystallite size (Å)	mean grain size (nm)	mean roughness height (nm)
SnS: undoped	125	37.7 ± 3.8	155 ± 27
SnS: In 3 %	116	61,0 ± 9.2	193 ± 25
SnS: In 6 %	125	62.6 ± 6.8	196 ± 20
SnS: In 9 %	119	58.6 ± 6.5	203 ± 38

Absorbance

According to basic semiconductor equations the absorption coefficient, in case of direct transitions is proportional to:

$$\alpha \propto \frac{1}{h\upsilon}\left(h\upsilon - E_g\right)^{1/2} \tag{1}$$

where h is Planck constant, ν is the frequency of incident photons and E_g is the bandgap energy. In case of indirect allowed transitions, the absorption coefficient is proportional to:

$$\alpha \propto \frac{1}{h\upsilon}\left(h\upsilon - E_g \pm E_{ph}\right)^{1/2} \tag{2}$$

where E_{ph} is the energy of phonons, the plus sign relates to the phonon absorption and minus to phonon emission. Thus the extrapolation of the straight part of either $(\alpha h\nu)^2$ or $(\alpha h\nu)^{1/2}$ vs $h\nu$ (assuming $E_{ph}<<E_g$) provides the bandgap energy of a semiconductor. Figure 3 presents a

plot, which allows identifying a direct transition. As we were unable to precisely determine the thickness of the layers, the absorption coefficient (α) is replaced here by total absorption (A).

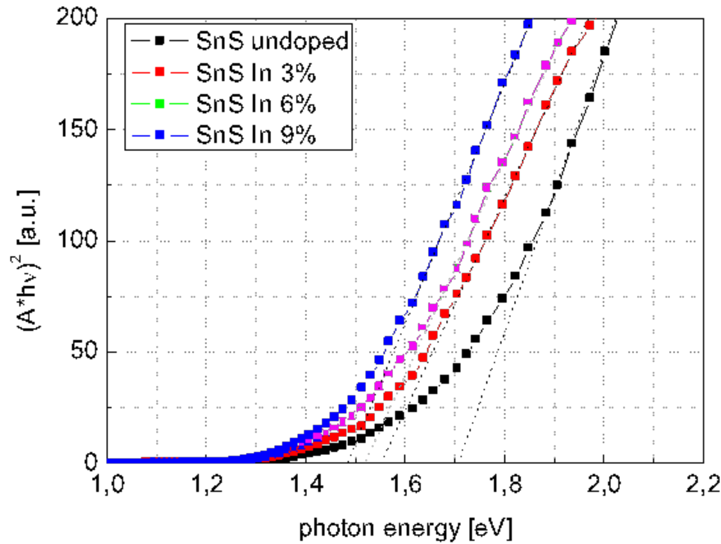

Figure 3. Plot of $(Ah\nu)^2$ versus photon energy $h\nu$ of SnS films with different In concentration. Extrapolation of the straight part of the plot is included with dotted lines.

The direct bandgap energies depend on the In concentration in the sprayed solution and decrease from 1.71 eV in case of undoped film to 1.48 eV for the film prepared with 9% concentration of In (Table 2). This is consistent with the available data on SnS thin films which mostly reports it as a direct bandgap semiconductor with bandgap energies around 1.5 eV [10, 12, 16]. This effect has already been observed [12] and explained by effective bandgap narrowing due to increased shallow acceptor concentration and formation of a defect intermediate energy band close to the valence band. However, this effect starts to be significant when carrier concentrations approach atomic concentrations and was observed i.e. in heavily doped ZnO [17]. This is not the case of investigated SnS samples, as their conductivity did not indicate such high carrier concentrations. The other reason of the lower bandgap in the In doped SnS might be at least twofold. The band structure of the material can change with addition of In and this will directly change the bandgap energy. However, the XRD data shows the same crystal structure of the material in all the samples. This implies no significant changes also in the band structure. The second reason might be related to the fact that the films were made in a non-vacuum process making incorporation of oxygen possible. It has been previously observed that the presence of oxygen widens the bandgap of the SnS [18]. The In might reduce incorporation of the oxygen atoms resulting in the lower bandgap of the SnS. It can be noted that the fitting was made here for the energies above 1.6 eV. The $(Ah\nu)^{1/2}$ vs $h\nu$ plot and a fitting made for lower energies reveals an indirect transition of around 1.05 eV independent on In concentration (Figure 4). It agrees well with the theoretical calculations of the SnS band structure, which indicates indirect bandgap energy of 1.07 eV [6].

Table 2. Energies obtained from extrapolating the straight part of the appropriate plots for direct and indirect transitions for SnS films with different In concentration

[In]/[Sn] ratio (%)	Direct transition energy (eV)	Indirect transition energy (eV)
0	1.71 ± 0.13	1.05 ± 0.03
3	1.55 ± 0.09	1.04 ± 0.03
6	1.52 ± 0.11	1.06 ± 0.04
9	1.48 ± 0.09	1.09 ± 0.04

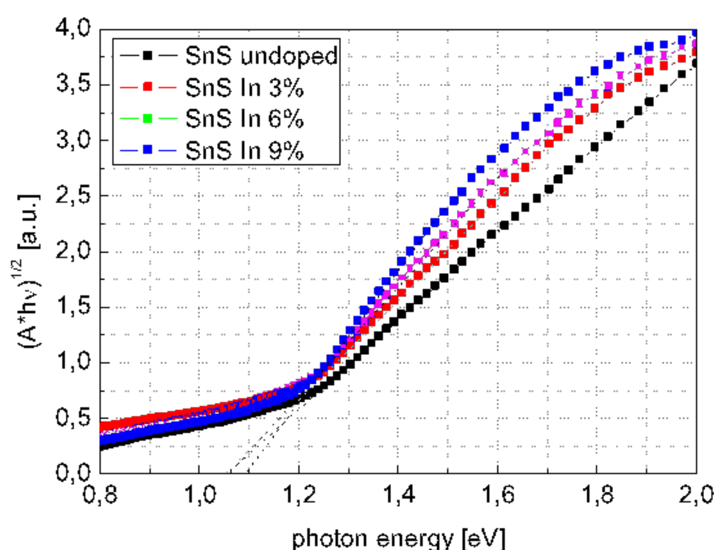

Figure 4. Plot of $(Ah\nu)^{1/2}$ versus photon energy hν of SnS films with different In concentration. Extrapolation of the straight part of the plot is included with dotted lines.

Photoluminescence

Photoluminescence is a widely used method to study defects in semiconductors by analysis of radiative recombination processes. Figure 5a shows a PL spectrum of an undoped SnS thin film measured at 10 K. The spectrum is a superposition of two radiative processes, labeled on the Figure 5a as (1) and (2). Fittings made with two Gaussian distributions give energies of observed radiative processes around E_A=1.1 eV and E_B=1.24 eV. The In doping does not change the shape of the PL spectrum significantly (Figure 5b). A 20 meV shift is observed in the sample with 9% of indium but in other cases, the change was negligible. There is also a change in the low energy part but looking at all the samples, these changes did not follow any systematic trend.

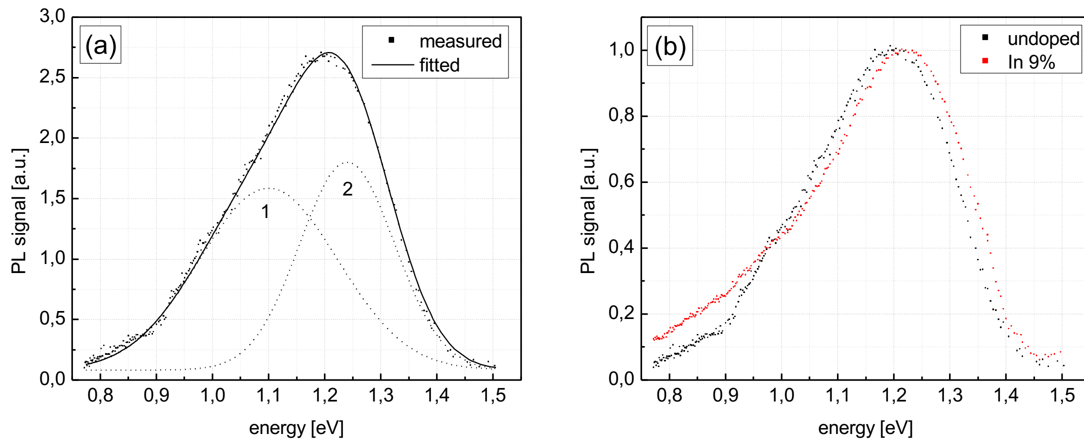

Figure 5. (a) A Photoluminescence spectrum of an undoped SnS thin film measured at 10K. Fitting with two Gaussian functions (1 and 2) is included on the graph. (b) Comparison of PL spectra for an undoped SnS layer and a SnS layer prepared with 9% of indium in the solution. The spectra are normalized to unity for the clarity.

The luminescence intensity I_{PL} follows a power law dependence on the excitation intensity I_{ex}:

$$I_{PL} = A * I_{ex}{}^{\gamma} \tag{3}$$

where A and γ are constants. It has been found that the type of the transition can be identified by the value of γ parameter with $\gamma<1$ indicating a donor to acceptor transition, $\gamma=1$ - free to bound transitions and $1<\gamma<2$ - the exciton-like transitions [19]. Figure 6 shows a PL intensity dependence on the excitation power. Fitting with a power law dependence (Equation 3) give the parameter $\gamma=0.54 \pm 0.08$ which points into donor to acceptor (DA) transitions.

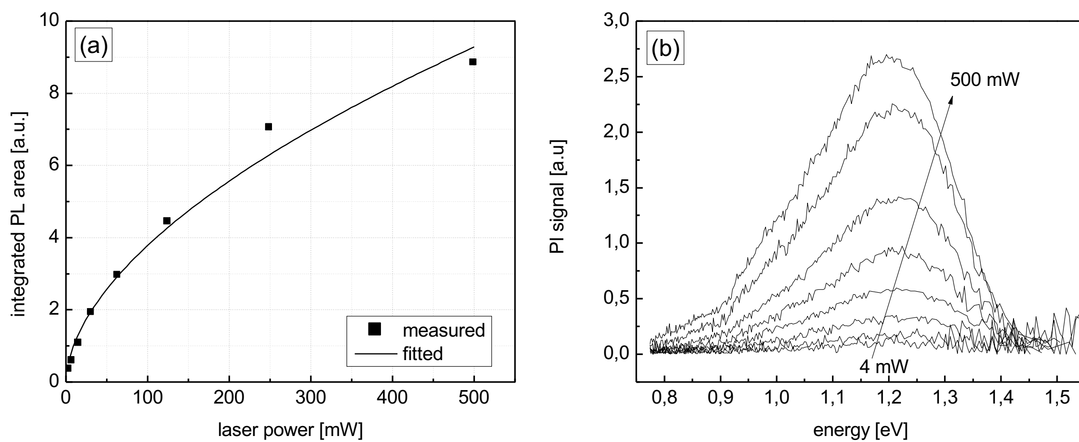

Figure 6. (a) Integrated area of Pl spectra measured at 10 K as a function of laser power. Fitting was made with power law dependence (Equation 3) and is included on the graph. (b) Complete PL spectra in the 4 mW – 500 mW laser power range.

To determine defect thermal activation energies temperature dependent measurements were performed. With increased temperature, the process of thermal emission from a defect level to the nearest band becomes more probable than the recombination and the intensity of PL decreases. The activation energy of a defect can be then calculated from quenching of the PL signal according to [20]:

$$PL \propto \frac{1}{1+T^{3/2}\sum_{i=1} a_i e^{-eE_{ai}/k_B T}} \tag{4}$$

where a_i is constant including a capture cross-section, E_{ai} is a thermal activation energy of a defect and k_B is a Boltzmann constant. The quenching of two identified DA transitions is shown on the Figure 7 together with the PL spectra at different temperatures.

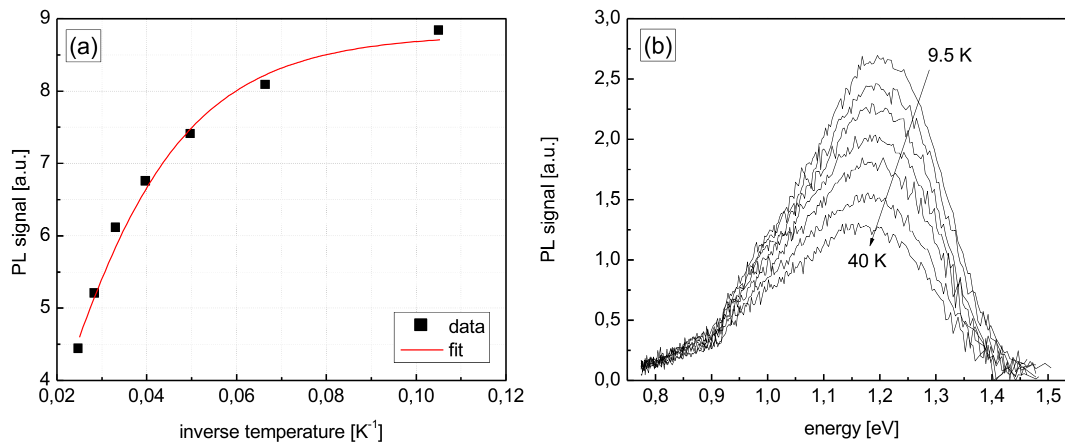

Figure 7. (a) Quenching of PL intensity for two observed donor acceptor transitions with increasing temperature. Fittings made using Equation (4) are included on the graph. (b) Complete PL spectra recorded in 9.5 K – 40 K temperature range.

Fittings made using Equation (4) gave in both cases one thermal activation energy, which is the activation energy of a shallower defect taking part in the donor-acceptor recombination process. We have obtained the following values of E_{a1}= 85±11 meV and E_{a2}= 93±13 meV. Taking into account the quality of the PL spectra and the quality of the fit itself, we conclude that in both transitions one of the defect levels taking part in the recombination process is the same and have thermal activation energy of 89±12 meV. The second defect must introduce in both cases a deep level because the sum of the activation energy and the transition energies is much lower than the bandgap value.

Conductivity measurements

Applicability of a material as an absorber in a solar cell requires not only good optical properties but also appropriate electrical conductivity. Figure 8 presents the electrical conductivity dependence on temperature of all investigated films. In temperatures above 200 K, the conductivity is thermally activated and follows exponential dependence on (1/T). Thus

the linear fitting to logarithm of conductivity versus (1/T) provides an activation energy (E_{act}) of conductivity, which in case of a p-type semiconductor is an energy distance from acceptor level (E_A) and the valence band $E_{act}=E_V-E_A$. The undoped SnS had activation energy of 164±2 meV and it does not change significantly except the case of sample with 9% of In concentration where value of 145±2 meV was obtained. Additionally slightly lower (160±2 meV) activation energy in layer with 6% In concentration may point into decreasing dependence of activation energy on In concentration. Taking into account the fact that the energy of a direct bandgap depends on the amount of indium in the solution this might mean that the energy position of the acceptor level responsible for the conductivity also changes when In is introduced.

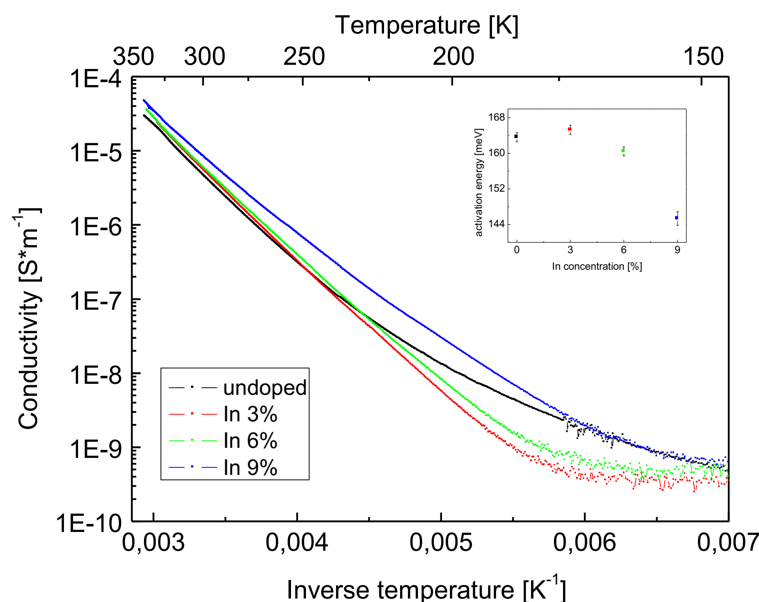

Figure 8. Electrical conductivity dependence on temperature for investigated series of thin films. The linear fittings were made in the same 250 K – 330 K temperature range for all the samples, providing activation energies included on the inset.

The conductivity at room temperature increases with increased amount of indium by factor of 1.78 between undoped SnS film and one doped with 9% of In. This might be a result of decreased activation energy. The observable decrease of activation energies should by itself give an increase of conductivity by factor of 2.1 ± 0.4.

Conclusions

In this work we presented the opto-electrical study of In doped SnS thin films made by spray pyrolysis. XRD analysis revealed orthorhombic structure with (111) dominant peak. AFM imaging show that films consist of longitudinal grains. The In doping slightly increase the roughness of the surface as well as the average size of the grains while the crystallite size remains constant. The material has an indirect bandgap with energy around 1.05 eV independent on In concentration. However, the absorption is dominated by the direct transition with energies decreasing with increased amount of indium from 1.71 eV to 1.48 eV.

The PL study revealed two donor to acceptor transitions independent on the In concentration. In both transitions, one of defect levels taking part in recombination process is common characterized by thermal activation energy of around 90 meV. However, our study did not allow us to judge whether the defect is a donor or an acceptor. The conductivity measurements show thermally activated conductivity with activation energies inversely dependent on In concentration in the 145 meV – 162 meV range. This decrease of activation energy results directly in higher conductivity of investigated thin films.

Acknowledgements

This work was supported by Ministerio de Economía y Competitividad (ENE2016-77798-C4-2-R) and Generalitat valenciana (Prometeus 2014/044).

References

[1] P. Jackson, D. Hariskos, R. Wuerz, O. Kiowski, A. Bauer, T.M. Friedlmeier, and M. Powalla, Properties of Cu(In,Ga)Se_2 solar cells with new record efficiencies up to 21.7%, Phys. Stat. Sol. (RRL) 9 (2015), pp. 28–31, doi:10.1002/pssr.201409520

[2] M. Gloeckler, I. Sankin and Z. Zhao, CdTe Solar Cells at the Threshold to 20% Efficiency, IEEE Journal of Photovoltaics 3, 4 (2013), pp. 1389-1393, doi:10.1109/JPHOTOV.2013.2278661

[3] K.T. Ramakrishna Reddy, N. Koteswara Reddy, R.W. Miles, Photovoltaic properties of SnS based solar cells, Solar Energy Materials and Solar Cells 90, 18–19 (2006), pp. 3041-3046, doi:/10.1016/j.solmat.2006.06.012

[4] L. Yu, S. Lany, R. Kykyneshi, V. Jieratum, R. Ravichandran, B. Pelatt, E. Altschul, H.A.S. Platt, J. F. Wager, D. Keszler, and A. Zunger, Iron Chalcogenide Photovoltaic Absorbers. Adv. Energy Mater. 1 (2011), pp. 748–753. doi:10.1002/aenm.201100351

[5] A. Ashour, The physical characteristics of Cu_2S/CdS thin-film solar cell, Journal of Optoelectronics and Advanced Materials 8.4 (2006), p. 1447

[6] J. Vidal, S. Lany, M. d'Avezac, A. Zunger, A. Zakutayev, J. Francis, J. Tate, Band-structure, optical properties, and defect physics of the photovoltaic semiconductor SnS, App. Phys. Lett. 100, 032104 (2012), doi:/10.1063/1.3675880

[7] W. Shockley, H. J. Queisser, Detailed Balance Limit of Efficiency of p-n Junction Solar Cells, Journal of Applied Physics 32 (1961), pp. 510-519, doi:/10.1063/1.1736034

[8] R. Jaramillo, V. Steinmann, C. Yang, K. Hartman, R. Chakraborty, J. R. Poindexter *et al.* Making Record-efficiency SnS Solar Cells by Thermal Evaporation and Atomic Layer Deposition. J. Vis. Exp. 99 (2015), p. 52705, doi:10.3791/52705

[9] N. Koteswara Reddy, K.T Ramakrishna Reddy, Growth of polycrystalline SnS films by spray pyrolysis, Thin Solid Films 325, 1–2 (1998), pp. 4-6, doi:/10.1016/S0040-6090(98)00431-3

[10] T. Sall, M. Mollar and B. Marí, Substrate influences on the properties of SnS thin films deposited by chemical spray pyrolysis technique for photovoltaic applications, J. Mater. Sci. 51 (2016), p. 7607, doi:10.1007/s10853-016-0039-9

[11] B.D. Malone, A. Galibc and E. Kaxirasad. First principles study of point defects in SnS, , Phys.Chem.Chem.Phys. 16 (2014), p. 26176, doi: 10.1039/c4cp03010a

[12] K. S. Kumar, C. Manoharan, S. Dhanapandian, A.G. Manohari, T. Mahalingam, Effect of indium incorporation on properties of SnS thin films prepared by spray pyrolysis, Optik - International Journal for Light and Electron Optics 125, 15 (2014), pp. 3996-4000, doi:/10.1016/j.ijleo.2014.01.144.

[13] H. Chaki Sunil, D. Chaudhary Mahesh, M.P. Deshpande, Effect of indium and antimony doping in SnS single crystals, Materials Research Bulletin, 63 (2015), pp. 173-180, doi:/10.1016/j.materresbull.2014.12.013.

[14] T.G. Hibbert, M.F. Mahon, K.C. Molloy, L.S. Price, I.P. Parkin, Deposition of tin sulfide thin films from novel, volatile (fluoroalkythiolato) tin (IV) precursors, J. Mater. Chem. 11 (2001), pp. 469–473

[15] J.I. Langford and A.J.C. Wilson, Scherrer after Sixty Years: A Survey and Some New Results in the Determination of Crystallite Size, *J. Appl. Cryst.* 11 (1978), pp. 102-113

[16] J.A. Andrade-Arvizu, M. Courel-Piedrahita, O. Vigil-Galán, SnS-based thin film solar cells: perspectives over the last 25 years, J. Mater. Sci. Mater. Electron. 26 (2015), p. 4541

[17] C. E. Kim et al., Effect of carrier concentration on optical bandgap shift in ZnO: Ga thin films, Thin Solid Films 518 (2010), pp. 6304-6307

[18] T. Sall, B. Marí Soucase, M. Mollar, B. Hartiti, M. Fahoume, Chemical spray pyrolysis of Β-In_2S_3 thin films deposited at different temperatures, J Phys Chem Solids 76 (2015), pp. 100–104

[19] J. I. Pankove, Optical Processes in Semiconductors (Dover Publications, New York, 1975).

[20] H. Shibata, Jpn. J. Appl. Phys. 37 (1997), p. 550